J. Fluid Mech. (2019), *vol.* 859, *pp.* 33–48.
doi:10.1017/jfm.2018.803

Instability and transition of a vertical ascension or fall of a free sphere affected by a vertical magnetic field

Jun-Hua Pan[1], **Nian-Mei Zhang**[1] **and Ming-Jiu Ni**[1,†]

[1]School of Engineering Science, University of Chinese Academy of Sciences, Beijing 101408, China

(Received 4 February 2018; revised 29 September 2018; accepted 5 October 2018;
first published online 16 November 2018)

When the Galileo number is below the first bifurcation, the instability and transition of a vertical ascension or the fall of a free sphere affected by a vertical magnetic field are investigated numerically. A compact model is used to explain that the magnetic field can destabilize the fluid–solid system. When the interaction parameter exceeds a critical value, the sphere trajectory is transitioned from a steady vertical trajectory to a steady oblique one. Furthermore, the trajectory will remain vertical at a sufficiently large magnetic field because of a double effect of the magnetic field on the fluid–solid system. Under the influence of an external vertical magnetic field, four wake patterns at the rear of the sphere are found and the physical behaviour of the free sphere is independent of the density ratio. The wake or trajectory of the free sphere is only determined by the Galileo number G and the interaction parameter N. A close relationship between the streamwise vorticity and the sphere motion is found. An interesting 'agglomeration phenomenon' is also found, which shows that the vertical velocities are agglomerated into a point for a certain magnetic field regardless of the Galileo number and satisfy a scaling law $V_z \sim N^{-1/4}$, when $N > 1$. The principal results of the present work are summarized in a map of regimes in the $\{G, N\}$ plane.

Key words: magnetohydrodynamics, materials processing flows, multiphase and particle-laden flows

1. Introduction

To understand the motion of a free particle under the simultaneous actions of gravity, buoyancy, hydrodynamic force and Lorentz force is one of the most important issues in magnetohydrodynamics (MHD) particle two-phase flows. An example in electromagnetic metallurgy is the production of clean metal, which excludes oxides and other types of non-metallic inclusions (El-Kaddah, Patel & Natarajan 1995). The other example is to produce an immiscible alloy with a uniform distribution of solid particles in the matrix (Zheng *et al.* 2015). Such a process can be modelled as the motion of free insulating particles in an MHD flow at rest at infinity. Therefore, understanding the influence of a magnetic field on the free insulating particle's motion can provide valuable knowledge for both the fundamental theory and practical applications.

† Email address for correspondence: mjni@ucas.ac.cn

Under the influence of an external magnetic field, any movement of a conducting fluid which is non-parallel to the magnetic field will generate electric currents. Consequently, these currents will interact with the magnetic field to create the Lorentz force (Davidson 2001), which can greatly modify the flow dynamics. MHD flow is characterized by two dimensionless parameters. One is the Reynolds number, which represents the ratio of inertial to viscous forces. The other is the interaction parameter, which gives a measurement of the ratio of electromagnetic to inertial forces. Many studies have investigated liquid metal flows past obstacles, such as magnetic obstacles (Cuevas, Smolentsev & Abdou 2006), square cylinders (Mück *et al.* 2000), cylinder cases with various directions of magnetic field (Lahjomri, Capéran & Alemany 1993; Mutschke *et al.* 2001; Kanaris *et al.* 2013) and sphere cases with theoretical (Goldsworthy 1961), experimental (Yonas 1967) or numerical (Pan, Zhang & Ni 2018) analyses. The work in Pan *et al.* (2018) investigated the wake structure and transition process of an incompressible viscous fluid flow past a fixed sphere affected by an imposed streamwise magnetic field, which found five wake structure patterns and their transitions behind a sphere at Reynolds numbers up to 300. Such an investigation will provide useful insight into the vortex dynamics of a freely moving body since the fixed sphere can be seen as a special case for which all its degrees of freedom are frozen.

When there is no magnetic field, a solid particle is generally modelled as a sphere and has been fully researched both in numerical simulations (Jenny, Dušek & Bouchet 2004; Zhou & Dušek 2015) and experiments (Veldhuis & Biesheuvel 2007; Horowitz & Williamson 2010). For such a free sphere motion, two control parameters are traditionally proposed to be of relevance. The first one is the density ratio $m = \rho_s/\rho$, where ρ_s and ρ are the density of the sphere and fluid, respectively. The second one is the non-dimensional number characterizing the ratio of buoyant and viscous effects, called the Galileo number G, which replaces the Reynolds number in the moving body case. It is defined as $G = U_0 d/\nu$ and U_0 is the gravitational velocity scale $U_0 = \sqrt{|m-1|gd}$, where g, d and ν are the acceleration due to gravity, the sphere diameter and the kinematic viscosity of the fluid, respectively. The Galileo number G governs the development of wake instabilities behind the sphere and the density ratio m governs the motion of the sphere in response to these flow instabilities and vortex-induced forces. Apart from these two parameters, recently, Mathai *et al.* (2017, 2018) reported that the onset of path instability was closely linked to the rotation of the sphere and the moment of inertia could significantly affect the trajectories, especially in flutter or tumble motion situations. Jenny *et al.* (2004) and Horowitz & Williamson (2010) found a primary bifurcation at about $G = 156$ or $Re = 210$, at which the trajectory of the sphere was transitioned from a steady vertical state to a steady oblique state. Fabre, Tchoufag & Magnaudet (2012) also analysed this bifurcation theoretically and remarked that this primary, regular bifurcation was independent of the density ratio. However, the threshold of the secondary bifurcation leading to unsteadiness is strongly dependent on the density ratio. The density ratio characterizes different trajectory regimes and their corresponding oscillation frequencies. As in recent works of Mathai *et al.* (2017, 2018), the moment of inertia can also significantly affect the trajectory of the sphere. With further increasing G, the trajectory is transitioned to chaos. The representation of different trajectory regimes in a $\{m, G\}$ plane can be referenced in detail in Jenny *et al.* (2004) or Zhou & Dušek (2015).

When an external magnetic field is concerned, another dimensionless parameter, the interaction parameter $N = (\sigma d B^2/\rho U_0)$ (Davidson 2001), needs to be considered.

Here, σ is the electrical conductivity and B is the magnetic field intensity. Now the different sphere trajectories are controlled by a three-dimensional parameter space $\{m, G, N\}$. As far as the authors know, although the vortex dynamics and motion of a free insulating particle under the influence of a magnetic field are important in the metallurgical industry, however, few available references have been published until now. Ern *et al.* (2012) reported that the particle trajectory is determined by its wake structure. However, liquid metal is opaque. Any optical method to visualize the vortex dynamics behind the sphere is useless, such as dye visualization or PIV technology. Therefore, three-dimensional numerical simulation is adopted. However, fully understanding the parameter space $\{m, G, N\}$ in the case of a freely moving sphere is a huge task, and the present manuscript tries to figure out part of it with the direct numerical simulation method.

Global linear stability analysis in Tchoufag, Fabre & Magnaudet (2014) showed that two types of models existed in a system involving a fluid–solid interaction, which caused the path instability. One is the solid model. It is related to an evolution of fluid–solid interaction when a disturbance is applied to the body's degrees of freedom. The other is the fluid model, which involves the wake instability that occurs beyond a critical Galileo number. Compared with the solid model, the fluid model does not require any coupling with the degrees of freedom of the body. As an external magnetic field is imposed, the interaction between the magnetic field and these two models will be complex. The present manuscript restricts our attention to the interaction between the magnetic field and the solid model. A vertical ascension or fall of a free sphere with the Galileo number less than 156 is chosen. Since the Galileo number is below the first bifurcation, the sphere will go along the vertical trajectory independent of the density ratio and no wake instability exists (Jenny *et al.* 2004; Zhou & Dušek 2015). After the sphere attains its stable state, an external vertical magnetic field is imposed to investigate two main questions: whether the vertical trajectory will be affected, and whether the trajectory is also independent of the density ratio.

2. Numerical method

The fluid–solid system of a sphere moving freely in a surrounding fluid is mathematically described by an explicit coupled system of Navier–Stokes and Newton motion equations. The flow velocity is expressed with respect to a fixed frame, but projected onto a translationally moving frame attached to the sphere centre of mass (Jenny & Dušek 2004). For most cases of liquid metal flow in industrial applications, the magnetic Reynolds number is very small. A so-called quasistatic approximation (Davidson 2001; Moreau 2013) of the MHD equations is invoked. The non-dimensional MHD equations governing the flow can be written as

$$\frac{\partial \boldsymbol{u}}{\partial t} + [(\boldsymbol{u} - \boldsymbol{v}_s) \cdot \nabla]\boldsymbol{u} = -\nabla p + \frac{1}{G}\nabla^2 \boldsymbol{u} + N(\boldsymbol{J} \times \boldsymbol{B}), \tag{2.1}$$

$$\nabla \cdot \boldsymbol{u} = 0, \tag{2.2}$$

$$\boldsymbol{J} = -\nabla \phi + \boldsymbol{u} \times \boldsymbol{B}, \tag{2.3}$$

$$\nabla \cdot \boldsymbol{J} = 0. \tag{2.4}$$

With the solenoidal current field (2.4) and Ohm's law (2.3), a Poisson equation for the electric potential can be derived as

$$\nabla \cdot \nabla \phi = \nabla \cdot (\boldsymbol{u} \times \boldsymbol{B}). \tag{2.5}$$

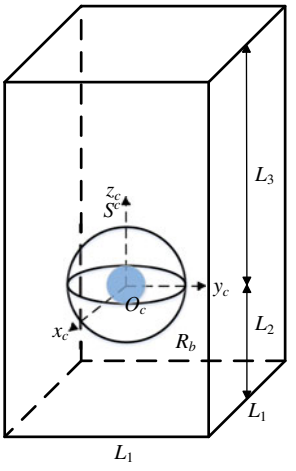

FIGURE 1. (Colour online) Geometry configuration for a freely moving sphere. The co-moving frame S^c is attached to the sphere centre of mass and has the same translation velocity $\boldsymbol{v}_s$. Some geometrical parameters are $L_1 = 16d$, $L_2 = 12d$, $L_3 = 25d$, and the radius of the spherical subdomain $R_b = 3d$. This subdomain is divided with an 'O' type grid.

The dimensionless flow variables, such as time t, velocity $\boldsymbol{u}$, pressure p, current density $\boldsymbol{J}$, imposed magnetic field $\boldsymbol{B}$ and electric potential ϕ are scaled with d/U_0, U_0, ρU_0^2, $\sigma U_0 B$, B and $dU_0 B$, respectively. The fluid–solid system has to be coupled by the no-slip boundary condition on the sphere surface Γ:

$$\boldsymbol{u}_\Gamma = \boldsymbol{v}_s + \boldsymbol{\Omega}_s \times \boldsymbol{r}_\Gamma, \tag{2.6}$$

where $\boldsymbol{r}$ denotes the position vector. The sphere velocity $\boldsymbol{v}_s$ and rotation velocity $\boldsymbol{\Omega}_s$ satisfy the non-dimensional Newton motion equations

$$m\frac{\mathrm{d}\boldsymbol{v}_s}{\mathrm{d}t} = \frac{6}{\pi}\boldsymbol{F}_\Gamma + \boldsymbol{i}, \quad \boldsymbol{F}_\Gamma = \int_\Gamma \boldsymbol{\tau}\cdot\boldsymbol{n}\,\mathrm{d}S, \tag{2.7a,b}$$

$$m\frac{\mathrm{d}\boldsymbol{\Omega}_s}{\mathrm{d}t} = \frac{60}{\pi}\boldsymbol{M}_\Gamma, \quad \boldsymbol{M}_\Gamma = \int_\Gamma \boldsymbol{r}\times\boldsymbol{\tau}\cdot\boldsymbol{n}\,\mathrm{d}S, \tag{2.8a,b}$$

where $\boldsymbol{n}$ is the outward normal direction of the boundary. The stress component is given as $\tau_{i,j} = -p\delta_{i,j} + (2/G)(\partial_i u_j + \partial_j u_i)$ and the force of the gravity and buoyancy $\boldsymbol{i} = \mathrm{sgn}(m-1)\boldsymbol{g}/g$.

Figure 1 shows the geometry configuration for the freely moving sphere. Since the grid moves translationally with the sphere velocity $\boldsymbol{v}_s$, the sphere is fixed relative to the grid. Therefore a consistent and conservative method in Ni *et al.* (2007) and the mesh resolution issue of a flow past a fixed sphere in Pan *et al.* (2018) can be re-used here. Then, a second-order leapfrog method (Dullweber, Leimkuhler & McLachlan 1997) is used for the six degrees of freedom solid body motion. Such explicit fluid–solid coupling is unstable when the added mass of the fluid is larger than the mass of the particle (Hu, Patankar & Zhu 2001). Here, a virtual force implementation (Schwarz, Kempe & Fröhlich 2015) is adopted for light particles. It is noted that for a rising or falling case, an identical grid is used with only a difference in the orientation of the gravity. Its direction is downward for a heavy sphere or upward for

Cases	$G=173$, $m=0.89$	$G=200$, $m=0.5$	$G=199$, $m=2.5$	$G_{max}=150$, $m=0.5$, $N_{max}=10$
Jenny *et al.* (2004)	$St=0.04$	$f=0.034$	—	—
Zhou & Dušek (2015)	—	$f=0.035$	$f=0.07$	—
Present work	$St=0.04$	$f=0.035$	$f=0.072$	$Vz=0.68$; $Vz=0.68$ (fine mesh)

TABLE 1. The verification of the present fluid–solid method. The grid resolution of extreme parameter at $G_{max}=150$ and $N_{max}=10$ is tested with a fine mesh. St, f and V_z are the Strouhal number, the oscillation frequency and the vertical velocity, respectively. Here, the Strouhal number is calculated as $St=fd/U_0$ and f, V_z are scaled with U_0/d and U_0, respectively.

Items	T	u_h	u_z	λ	R	C_d
Zhou & Dušek (2015)	9.22	0.326	1.501	13.8	0.48	0.59
Present work	9.53	0.359	1.476	14.0	0.54	0.58

TABLE 2. The comparison for a free spirally rising sphere at $G=500$, $m=0.1$. Here, T, u_h, u_z, λ, R and C_d are the period, horizontal velocity, vertical velocity, spiral pitch, spiral radius and drag coefficient, which are scaled with d/U_0, U_0, U_0, d, d and $(1/2)\rho U_0^2$, respectively.

a light sphere, so the sphere will always move from up to down. Hence, the bottom wall of the domain physically corresponds to a infinitely far boundary and here the velocity and pressure gradient are set to be zero. A convective boundary condition is applied at the top wall while the other side walls are set with a slip boundary condition. A no-slip boundary condition is imposed on the sphere surface. For an MHD flow, the electric potential for all boundaries is set as

$$\frac{\partial \phi}{\partial n} = (\boldsymbol{u} \times \boldsymbol{B}) \cdot \boldsymbol{n}. \tag{2.9}$$

The above equation is derived by projecting the electric potential equation (2.5) on the boundary and it reduces to the requirement of charge conservation in the domain. The verification of the present fluid–solid method for ascension or fall of a free sphere is given in tables 1 and 2, which show that it can handle both light and heavy sphere cases.

3. Results

3.1. *Transition from a steady vertical trajectory to a steady oblique one*

When the Galileo number is below the first bifurcation and no magnetic field exists, a free sphere will travel with vertical trajectory regardless of the density ratio. No wake instability will occur and only the solid model exists in the fluid–solid system. A series of cases at $m=0.5$ with different Galileo numbers are first simulated to get their final stable states. Then an external vertical magnetic field is imposed. Figure 2 shows that the sphere with a steady vertical trajectory becomes steady oblique. Obviously, the instability occurs with an external vertical magnetic field. Generally, the magnetic field will play a damping role in a free rising bubble with an oscillatory path, as reported in experiment (Zhang, Eckert & Gerbeth 2005) and simulation (Zhang & Ni 2017). They reported that an external vertical magnetic field

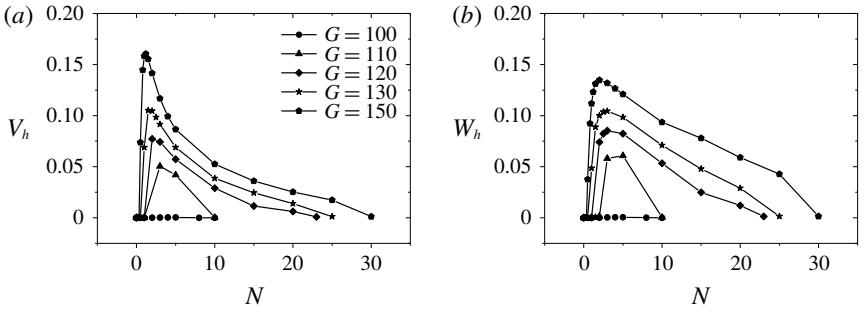

FIGURE 2. Horizontal velocity V_h and rotation velocity W_h of the sphere at $m = 0.5$ with different Galileo numbers versus the interaction parameter. The V_h, W_h are scaled with U_0 and U_0/d, respectively. (*a*) Horizontal velocity. (*b*) Horizontal rotation velocity.

was used to diminish the asymmetry of the vertical vortex pairs. It is noted that the wake structure behind the bubble determines its trajectory (Ern *et al.* 2012) and more symmetric vertical vortex pairs will lead to a more stable trajectory. Hence, their results showed that the oscillatory path of a bubble was transitioned to a more rectilinear trajectory. The oscillatory bubble mainly relates to the fluid model, which involves the wake instability. However, the present fluid–solid system only has the solid model and figure 2 shows that the interaction between the magnetic field and the solid model facilitates the transition onset here.

A weakly nonlinear expansion method in Fabre *et al.* (2012) reported that the horizontal rotation played a key role in the transition onset from a steady vertical trajectory to a steady oblique one without a magnetic field. Hence, some numerical experiments are designed about rotation degrees of freedom at $G = 150$, $m = 0.5$ with different interaction parameters. As shown in figure 2, when $N > N_c \approx 0.4$, the transition occurs and a horizontal velocity exists. Figure 3(*a*,*b*) shows comparison results by freezing all rotation degrees of freedom of the sphere. No horizontal velocity occurs at a small magnetic field $N = 0.5$, while there is a transition onset at a large magnetic field $N = 2$. These results indicate that both the rotation and the translation degrees of freedom can facilitate the transition onset and the rotation one plays a key role, which agrees with the conclusions found without a magnetic field in Jenny, Bouchet & Dušek (2003) and Fabre *et al.* (2012). Furthermore, a 1 % perturbation of horizonal rotation velocity at $N = 0.5$ is added on the sphere with different interaction parameters. Figure 3(*c*) shows that the perturbation is suppressed when $N < N_c$ or it is quickly enlarged when $N > N_c$. These results imply that the perturbation can only grow when the magnetic field is beyond a critical value N_c.

Relative to the reference frame which is fixed in the centre of the sphere and has the same translation velocity $\boldsymbol{v}_s$, the original free motion with $G < 156$ in the absence of a magnetic field is equivalent to a flow past a fixed sphere, for which the flow is steady and axisymmetric and a separated bubble is attached at the rear of the sphere. After the fluid–solid system reaches its stable state, an external vertical magnetic field is imposed. A diagram in figure 4(*a*) shows that the flow field is affected by the magnetic field. With some vector operations, equation (2.5) can be reformed as $\nabla \cdot \nabla\phi = \nabla \cdot (\boldsymbol{u} \times \boldsymbol{B}) = \boldsymbol{B} \cdot \omega = 0$, since the flow is axisymmetric and no vertical vorticity exists. So ϕ is zero (or a constant) and no current is induced from the electric potential in Ohm's law (2.3). The Lorentz force can be rewritten as $\boldsymbol{F}_L = -N\boldsymbol{u}_\perp B^2$, which always prevents the flow that is not parallel to the magnetic

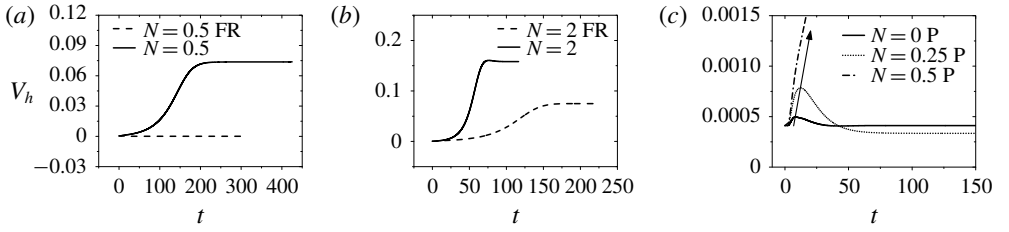

FIGURE 3. Numerical experiments at $G = 150$, $m = 0.5$ affected by a magnetic field. 'FR' and 'P' stand for 'freeze rotation' and 'perturbation', respectively. The V_h and time are scaled with U_0 and d/U_0, respectively. (*a*) Freeze all rotation degrees of freedom at $N = 0.5$. (*b*) Freeze all rotation degrees of freedom at $N = 2$. (*c*) A 1 % perturbation of horizonal rotation velocity at $N = 0.5$ is added on the sphere with different interaction parameters.

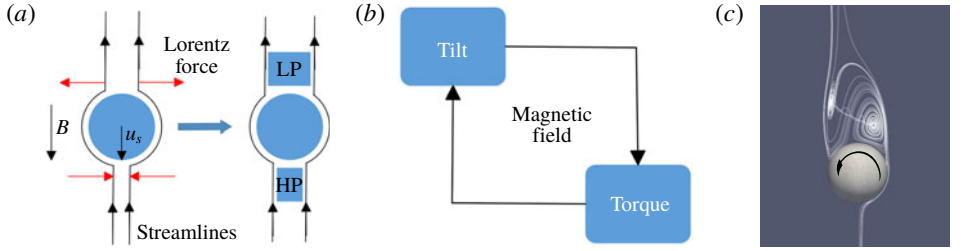

FIGURE 4. (Colour online) Understanding the transition onset of a horizonal velocity. (*a*) A compact model for the influence of the magnetic field. 'HP' and 'LP' stand for 'high pressure' and 'low pressure', respectively, due to the Lorentz force. The high pressure in the HP region pushes away the streamlines and the Lorentz force in the LP region directly pulls away the streamlines. (*b*) A positive feedback effect for the fluid–solid system. (*c*) Three-dimensional streamlines projected onto the symmetric plane at $Re = 250$ with $N = 0$ in a fixed sphere case.

field. Here, $\boldsymbol{u}_\perp$ represents the velocity components normal to $\boldsymbol{B}$. Due to the Lorentz force, two relatively stagnant regions ahead of and behind the sphere occur, as shown in figure 4(*a*). The streamlines compactly wrap the sphere without a magnetic field and now they are loosened by the Lorentz force. Consequently, the stability of the fluid–solid system is decreased. As implied in figure 3(*c*), increasing the magnetic field destabilizes the fluid–solid system and the transition occurs when the magnetic field exceeds a critical value N_c. Figure 2 indicates that the smaller the Galileo number of a case is, the larger the critical value it has. This is because a small Galileo number case has a smaller separated bubble (Johnson & Patel 1999). That is to say, the sphere is more compactly wrapped by the streamlines and it needs a larger magnetic field to decrease the stability of the fluid–solid system.

Assuming that one is at the centre of the sphere to observe the flow field, an axisymmetric recirculation exists behind the sphere. Jenny *et al.* (2003) reported that the instability of a free sphere degrees of freedom was associated with the azimuthal wave perturbations of the flow. When the stability of the fluid–solid system is decreased by the magnetic field ($N > N_c$), these perturbations will evolve and the axisymmetric recirculation is broken, which results in a small tilt shift of the recirculation. Actually, such a tilt corresponds to a torque on the original non-rotating

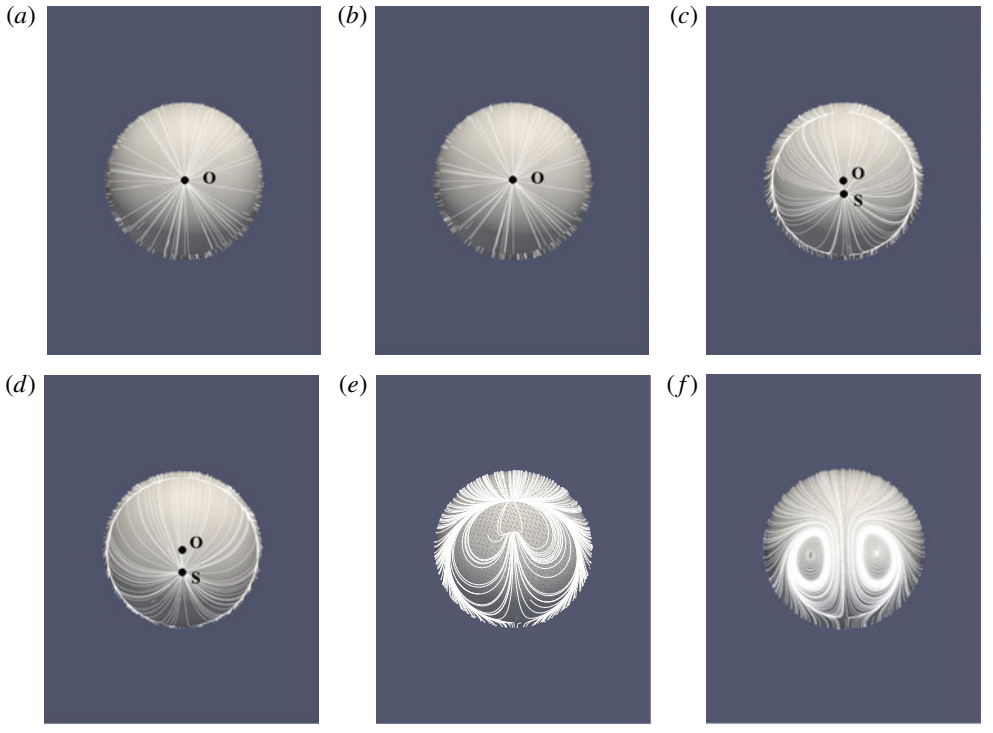

FIGURE 5. (Colour online) Four types of skin friction lines at $G = 150$, $m = 0.5$ affected by different interaction parameters. 'O' and 'S' indicate the centre of the sphere and the stagnation point, respectively. (*a*) $N = 0$. (*b*) $N = 0.25$, type I. (*c*) $N = 0.5$, type II. (*d*) Case comparison with $G = 165$, $m = 0.5$, $N = 0$. (*e*) $N = 1.2$, type III. (*f*) $N = 2$, type IV.

sphere, as shown in figure 4(*c*). Such a torque can be fully compensated by the sphere rotation. Furthermore, the rotation of the sphere will enlarge the tilt of the recirculation, which will exert a net torque on the sphere. This net torque needs a larger rotating velocity of the sphere to compensate its effect. Finally, the sphere will stay in a new steady state, for which the hydrodynamic torque and lift remain zero. Hence, the positive feedback effect shown in figure 4(*b*) exists, which transitions the fluid–solid system into a new equilibrium state.

3.2. *The wake structures at the rear of the sphere*

The wake structures behind the sphere of figure 2 are analysed in detail in this section. Lighthill (1963) proposed that convergence of skin friction lines was a criterion of a three-dimensional flow separation. Skin friction lines can clearly show flow traces at the rear of the sphere, which help to visualize the wake structures. Figure 5 shows various wake structures affected by different interaction parameters.

When $N < N_c$, the transition onset does not occur. The wake structures behind the sphere are still axisymmetric, as shown in figure 5(*a*,*b*). Such an axisymmetric wake is unable to generate any side force on the sphere and the sphere rises vertically. Increasing the magnetic field, the compact model in figure 4(*a*) indicates that the stability of the fluid–solid system is decreased. Then a transition occurs when the magnetic field exceeds a critical value N_c and the fluid–solid system goes into a new

equilibrium state with a positive feedback effect in figure 4(*b*). If we stand on the centre of the sphere to observe the flow field (non-inertial frame), it has a similar wake structure with a flow past a fixed sphere at $210 < Re < 270$, as shown in figure 4(*c*). The topological structure of the streamlines has a small left spiral and large right spiral and they are tilted behind the sphere. The corresponding skin friction lines are shown in figure 5(*c*), which shows that the stagnation point shifts from the centre because of the tilt of the recirculation. Furthermore, figure 5(*d*) shows the same wake structure as figure 5(*c*), but without a magnetic field. Note that the first bifurcation is about $G = 156$ and the magnetic field shifts the transition onset into a lower critical threshold of the Galileo number. Ern *et al.* (2012) claimed the wake of the fixed sphere would provide useful insight into the vortex dynamics of the freely moving body. The wake structures of a flow past a fixed sphere affected by a streamwise magnetic field in Pan *et al.* (2018) or a transverse rotation of the sphere in Giacobello, Ooi & Balachandar (2009) indicated that both the left and right spirals in figure 4(*c*) can be dismissed by these two effects. So further increasing the magnetic field, figure 5(*e*) indicates that only the small left spiral disappears while both these two spirals disappear in figure 5(*f*). The detailed Lorentz force action on the two spirals can be found in Pan *et al.* (2018). As shown in figure 4, a positive feedback effect includes a transverse rotation of the sphere. The existence of the transverse rotation will facilitate the fluid–solid system to quickly change to a new equilibrium state, which can be seen in figure 3(*b*) compared with the case of no rotation.

As shown above, the rising sphere at $G = 150$ and $m = 0.5$ has four kinds of wake structures under the influence of a vertical magnetic field. Assume that one is at the centre of the sphere to observe the flow field. Since types I, II and III still have recirculation, the tilt of the recirculation will convert the azimuthal vorticity into a streamwise vorticity. With the existence of a positive feedback effect, by increasing the magnetic field, the tilt will increase quickly, which means that more streamwise vorticity is converted behind the sphere. When the flow pattern is in type IV, no recirculation exists, so the positive feedback effect is excluded. Now the Lorentz force always suppresses the streamwise vorticity and the intensity of the streamwise vorticity will decrease. Such a variation of the streamwise vorticity is shown in figure 6(*b*). Actually, the flow in type I is axisymmetric and no streamwise vorticity exists. The topological structures of the streamwise vorticity in types II, III and IV are the same. They are plane symmetric with a counter-rotating vortex pair, as shown in figure 6(*a*), which are only different in the intensity affected by the magnetic field. But the skin friction lines show four different topological structures, which implies more flow field information to analyse the fluid dynamics. Furthermore, figure 7 shows that the streamwise vorticity can induce an induced flow. With the law of interaction, a lift force corresponding to this induced flow will be produced in the symmetric plane, which will drive the sphere. Thus a horizontal velocity occurs to compensate the lift force. Since the magnitude of the force determines the horizontal velocity, the horizontal velocity has an identical variation trend to the streamwise vorticity, as shown in figures 6(*b*) and 8.

An interesting phenomenon in figure 8 is that the inflection point of the horizontal rotation velocity is $N = 2$, which is different from that of the horizontal velocity $N = 1.2$. The torque exerting on the non-rotating sphere is determined from the viscous stress force on the sphere surface, since the pressure force has no contribution. This torque is fully compensated by the sphere rotation. The tilt of skin friction lines at the rear of the sphere reflects the magnitude of viscous stress force and is closely related to the tilt of recirculation behind the sphere. As can be seen in figure 5, the tilt of

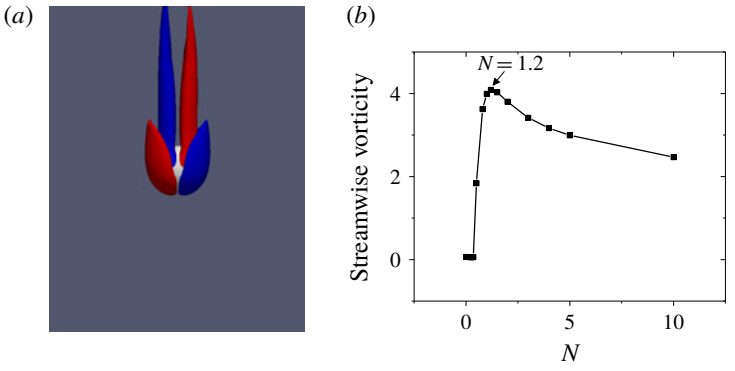

FIGURE 6. Streamwise vorticity behind the sphere at $G = 150$, $m = 0.5$ affected by a magnetic field. (a) The isosurfaces of streamwise vorticity with $\omega_z = \pm 0.4$ at $N = 2$ in a front view. (b) The maximal magnitude of streamwise vorticity affected by different interaction parameters.

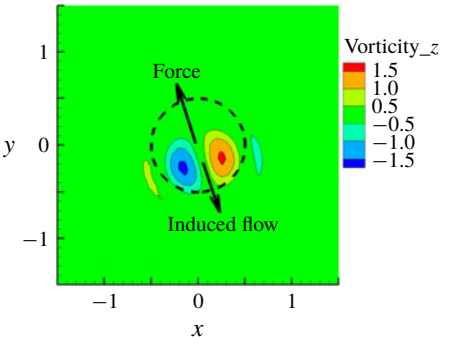

FIGURE 7. Cross-section plot of vertical vortical structures at $z = 1d$ behind the sphere with $G = 150$, $m = 0.5$, $N = 1.2$. The dashed line represents the sphere.

skin friction lines is increasing from type I to III, so the horizontal rotation velocity becomes large. However, it is not clear for type IV, since there is no recirculation behind the sphere. It is noted that the skin friction lines are in connection with the flow pattern behind the sphere. Hence, the tilt of the skin friction lines can be quantitatively measured by the angle θ between the vertical direction and the direction along the thread of streamwise vorticity, as shown in figure 9(a). Figure 9(b) plots the variation of angle θ affected by different magnetic fields, which determines the variation trend of the horizontal rotation velocity, as shown in figure 8.

In figure 6(b), when $N < 1.2$, the flow patterns are in regimes I, II and III. For such regimes, the magnetic field facilitates the transition onset and the positive feedback effect exists, which will make the streamwise vorticity change quickly. When $N > 1.2$, the flow pattern now is in regime IV, where no positive feedback effect exists and the Lorentz force always suppresses the streamwise vorticity and slowly decreases it. It is noted that the Lorentz force will damp a flow that is non-parallel to the magnetic field, which actually prevents the tilt of the recirculation. So there is competition between the suppression of the Lorentz force and the positive feedback effect on the tilt of recirculation behind the sphere. When the positive

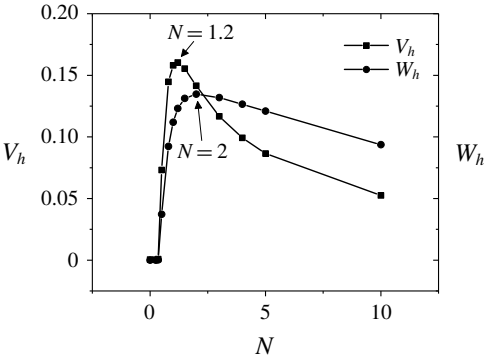

FIGURE 8. Horizontal velocity V_h and rotation velocity W_h of the sphere at $G = 150$, $m = 0.5$ affected by different interaction parameters. The V_h, W_h are scaled with U_0 and U_0/d, respectively.

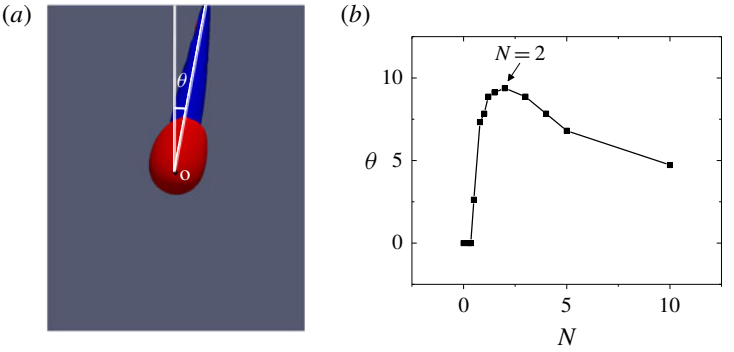

FIGURE 9. (Colour online) The angle θ between the vertical direction and the direction along the thread of streamwise vorticity at $G = 150$, $m = 0.5$ affected by a magnetic field. 'O' indicates the centre of the sphere. (*a*) The isosurfaces of streamwise vorticity with $\omega_z = \pm 0.4$ at $N = 2$ in a side view. (*b*) The angle θ affected by different interaction parameters.

feedback effect is dominant, the tilt is enlarged. With an increasing magnetic field, the suppression of the Lorentz force becomes strong enough to prevent the development of the tilt caused by the positive feedback effect. For the case $G = 110$, the fluid–solid system is more stable than the case of $G = 150$. With the competition between the suppression of the Lorentz force and the positive feedback effect, no wake in types III and IV occurs. In the present investigations, the free sphere first attains its stable state without a magnetic field, then an external vertical magnetic field is imposed. Furthermore, for a sufficiently large magnetic field, a perturbation creates a small tilt of the recirculation behind the sphere. Since the Lorentz force is large enough, it prevents the tilt of the recirculation and the positive feedback effect can not be evolved any longer. Now the wake will remain axisymmetric and no horizontal velocity exists. Such cases correspond to a sufficiently large magnetic field situation as in figure 2. It is interesting that the magnetic field has a double effect on the fluid–solid system, which will facilitate or prevent the tilt of the recirculation in term of different magnetic field intensities. For the case $G = 100$ in figure 2, considering the double effect of the magnetic field, on the one hand,

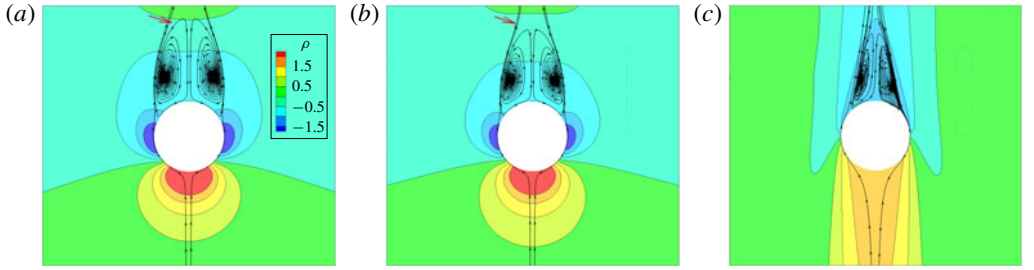

FIGURE 10. Pressure contours and streamlines in the symmetric plane at $G = 150$, $m = 0.5$ with different interaction parameters. The streamlines are plotted with the relative fluid velocity $\boldsymbol{u}_r = \boldsymbol{u} - \boldsymbol{v}_s$. The red arrow indicates the same position. (*a*) Without a magnetic field at $N = 0$. (*b*) Close to a critical magnetic field at $N = 0.35$. (*c*) With a sufficiently large magnetic field at $N = 30$.

it needs a larger magnetic field to facilitate transition onset because the sphere is more compactly wrapped by streamlines. On the other hand, this large magnetic field also plays a suppressing role and now the suppression of the large Lorentz force is more dominant than that of the positive feedback effect, which will prevent the tilt of the recirculation. Hence, no transition onset will occur and the horizontal velocity remains zero.

Figure 10 shows three kinds of typical axisymmetric flows at $G = 150$, $m = 0.5$, when the magnetic field is absent, close to a critical value, or sufficiently large. Here, the streamlines are plotted with the relative fluid velocity. It is assumed that one is at the centre of the sphere and observing the recirculation flow at the rear of the sphere. In figure 10(*a*,*b*), the streamlines at the position indicated by a red arrow are pulled away from the recirculation by the Lorentz force $\boldsymbol{F}_L = -N\boldsymbol{u}_\perp B^2$ and flow downstream. The sphere is compactly wrapped by streamlines at $N = 0$ and these streamlines are loosened by the Lorentz force, which will destabilize the fluid–solid system. A compact model is given to explain the transition onset in § 3.1. The pressure contour and streamlines in figure 10(*c*) are not perfectly symmetric. This is because the suppression of the large Lorentz force is more dominant than the positive feedback effect and a small tilt of the recirculation caused by a perturbation can not be evolved. Furthermore, the change of the recirculation bubble, such as recirculation length and separation angle affected by a magnetic field in a axisymmetric flow zone is similar to a flow past a fixed sphere case at $Re = 150$ in Pan *et al.* (2018).

3.3. *Independence of the density ratio*

The above results are relative to the density ratio $m = 0.5$. Fabre *et al.* (2012) reported the primary bifurcation was independent of the density ratio without a magnetic field. So now we check the role of the density ratio in the three-dimensional parameter space $\{m, G, N\}$. A wide density ratio m parameter space [0.01,10] with different Galileo numbers versus the interaction parameter are simulated. A total of 159 cases are simulated and the results show that the physical behaviour of the free sphere is also independent of the density ratio when affected by the magnetic field, regardless of whether there is a transition onset or not. The wake or trajectory of the freely moving sphere is only determined by the Galileo number and the interaction parameter. Hence, the parameter space $\{m, G, N\}$ can reduce to $\{G, N\}$, when $G < 156$. The results of

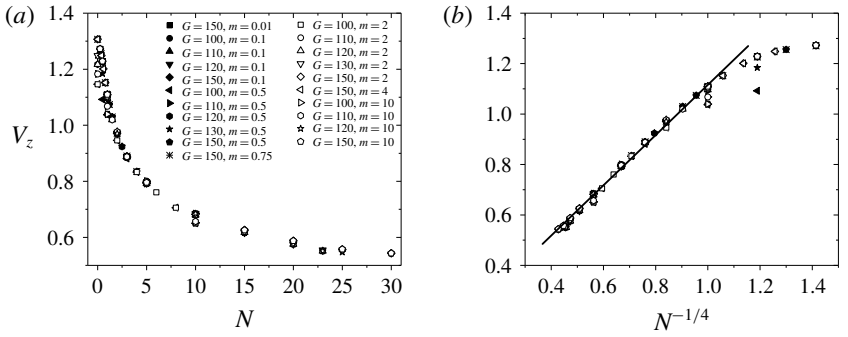

FIGURE 11. The vertical velocities of different Galileo numbers G and density ratios m. The V_z is scaled with U_0. (*a*) The vertical velocities are agglomerated into a point for a certain magnetic field, when $N > 1$. An agglomerated curve line consists of these points. (*b*) Linear dependence of the vertical velocity versus $N^{-1/4}$, when $N > 1$.

$m = 0.5$ in the above sections can be extended to any density ratio, so the results of other density ratios are not repetitively plotted. The independence of the density ratio can be easily understood in Newton motion equations (2.7) and (2.8). The sphere has a steady state in the final state. Thus the time derivative term disappears at last and the remaining equations are free of the density ratio.

The vertical velocity is also plotted in figure 11(*a*). It is clearly seen that when $N>1$, the vertical velocities of different Galileo numbers are agglomerated into a point for a certain magnetic field, which means that it is not only independent of the density ratio, but also the Galileo number. We call this the 'agglomeration phenomenon'. The vertical velocity in the final state is controlled by (2.7). It is simplified as

$$0 = \frac{6}{\pi}\int_{\Gamma} \boldsymbol{\tau}\cdot\boldsymbol{n}\,\mathrm{d}S\cdot\boldsymbol{e}_{\parallel} + \mathrm{sgn}(m-1). \tag{3.1}$$

Here, $\boldsymbol{e}_{\parallel}$ denotes the vertical direction. As in the analysis in figure 4(*a*), with the suppression of the Lorentz force, a high pressure zone and a low pressure zone will occur. Therefore, when affected by a strong magnetic field, the pressure drop contribution of the stress force $\tau_{i,j} = -p\delta_{i,j} + (2/G)(\partial_i u_j + \partial_j u_i)$ is dominant. The second term related to the Galileo number can be ignored. It is noted that for a small Galileo number, the contribution of the second term in stress force increases and the data point will have little deviation from the agglomerated curve line.

A simple drag law $C_d \propto N^{1/2}$ is found for the flow past a sphere affected by a strong streamwise magnetic field (Pan *et al.* 2018). The law is also suitable for the present research if we stand on the sphere centre to observe the flow field. In the vertical direction, the balanced relation among the drag force, gravity and buoyancy gives the formula

$$\sqrt{N}\cdot\tfrac{1}{2}\rho u_z^2\cdot\pi R^2 \sim |\rho_s-\rho|\cdot\tfrac{4}{3}\pi R^3\cdot g, \tag{3.2}$$

where R is the sphere radius. Substitute the dimensionless vertical velocity $V_z = u_z/U_0$ into the equation and simplify it to get a scaling law:

$$V_z \sim N^{-1/4}. \tag{3.3}$$

The data points in figure 11(*a*) are replotted in figure 11(*b*). It is clearly seen that the vertical velocity is linear dependent on $N^{-1/4}$, when $N > 1$.

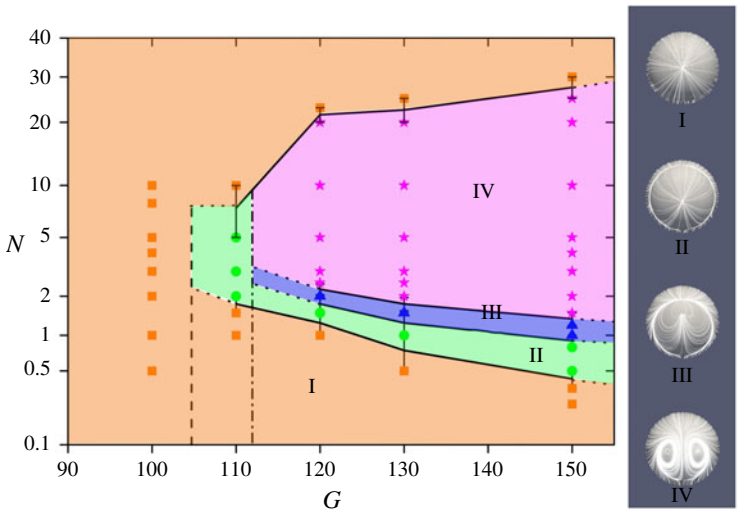

FIGURE 12. Map of regimes for wake patterns at the rear of the sphere in the $\{G, N\}$ plane. Assume that one is at the centre of the sphere to observe the flow field in the rear of the sphere. Regime I is the steady axisymmetric state with an attached separation bubble. The pattern in regime II is the steady plane symmetric with small and large spirals in the recirculation region. Regimes III and IV are also steady plane symmetric, for which the small spiral in regime III disappears and both small and large spirals disappear in regime IV. □, ◇, △ and ⋆ represent calculated data points.

4. Summary

The present study is undertaken with the objective of numerically simulating and analysing in detail the instability and transition of a vertical ascension or fall of a free sphere under the influence of an imposed external vertical magnetic field. The magnetic field can decrease the stability of the fluid–solid system and the trajectory will be transitioned from a steady vertical trajectory to a steady oblique one if the interaction parameter exceeds a critical value. At the same time, the double effect of a sufficiently large magnetic field on the fluid–solid system can preserve the sphere's steady vertical trajectory. In order to define the various wake structures and the transition processes, a total of 159 cases in the parameters' space $\{m, G, N\}$ are performed. We find that the physical behaviour of the free sphere is independent of the density ratio. Only the Galileo number and the interaction parameter determine the wake or trajectory of the sphere. A map of regimes consisting of four wake patterns at the rear of the sphere in the $\{G, N\}$ plane is given in figure 12. There is a close relationship between the streamwise vorticity and the sphere motion. The magnitude of the streamwise vorticity determines the horizontal velocity of the sphere while the angle θ between the vertical direction and the direction along the thread of streamwise vorticity determines the sphere horizontal rotation velocity. A so-called 'agglomeration phenomenon' is found, which describes the vertical velocities of different Galileo numbers that are agglomerated into a point for a certain magnetic field. This means that the vertical velocity is not only independent of the density ratio, but also of the Galileo number. Furthermore, when $N > 1$, the vertical velocity satisfies a scaling law $V_z \sim N^{-1/4}$.

Acknowledgements

The authors gratefully acknowledge the support from NSFC (grants 51636009 and 51776194) and from CAS (grant XDB22040201).

REFERENCES

CUEVAS, S., SMOLENTSEV, S. & ABDOU, M. A. 2006 On the flow past a magnetic obstacle. *J. Fluid Mech.* **553**, 227–252.

DAVIDSON, P. A. 2001 *An Introduction to Magnetohydrodynamics*. Cambridge University Press.

DULLWEBER, A., LEIMKUHLER, B. & MCLACHLAN, R. 1997 Symplectic splitting methods for rigid body molecular dynamics. *J. Chem. Phys.* **107** (15), 5840–5851.

EL-KADDAH, N., PATEL, A. D. & NATARAJAN, T. T. 1995 The electromagnetic filtration of molten aluminum using an induced-current separator. *JOM J. Miner. Met. Mater. Soc.* **47** (5), 46–49.

ERN, P., RISSO, F., FABRE, D. & MAGNAUDET, J. 2012 Wake-induced oscillatory paths of bodies freely rising or falling in fluids. *Annu. Rev. Fluid Mech.* **44**, 97–121.

FABRE, D., TCHOUFAG, J. & MAGNAUDET, J. 2012 The steady oblique path of buoyancy-driven disks and spheres. *J. Fluid Mech.* **707**, 24–36.

GIACOBELLO, M., OOI, A. & BALACHANDAR, S. 2009 Wake structure of a transversely rotating sphere at moderate Reynolds numbers. *J. Fluid Mech.* **621**, 103–130.

GOLDSWORTHY, F. A. 1961 Magnetohydrodynamic flows of a perfectly conducting, viscous fluid. *J. Fluid Mech.* **11** (4), 519–528.

HOROWITZ, M. & WILLIAMSON, C. H. K. 2010 The effect of Reynolds number on the dynamics and wakes of freely rising and falling spheres. *J. Fluid Mech.* **651**, 251–294.

HU, H. H., PATANKAR, N. A. & ZHU, M. Y. 2001 Direct numerical simulations of fluid–solid systems using the arbitrary Lagrangian–Eulerian technique. *J. Comput. Phys.* **169** (2), 427–462.

JENNY, M., BOUCHET, G. & DUŠEK, J. 2003 Nonvertical ascension or fall of a free sphere in a Newtonian fluid. *Phys. Fluids* **15** (1), L9–L12.

JENNY, M. & DUŠEK, J. 2004 Efficient numerical method for the direct numerical simulation of the flow past a single light moving spherical body in transitional regimes. *J. Comput. Phys.* **194** (1), 215–232.

JENNY, M., DUŠEK, J. & BOUCHET, G. 2004 Instabilities and transition of a sphere falling or ascending freely in a Newtonian fluid. *J. Fluid Mech.* **508**, 201–239.

JOHNSON, T. A. & PATEL, V. C. 1999 Flow past a sphere up to a Reynolds number of 300. *J. Fluid Mech.* **378**, 19–70.

KANARIS, N., ALBETS, X., GRIGORIADIS, D. & KASSINOS, S. 2013 Three-dimensional numerical simulations of magnetohydrodynamic flow around a confined circular cylinder under low, moderate, and strong magnetic fields. *Phys. Fluids* **25** (7), 074102.

LAHJOMRI, J., CAPÉRAN, P. & ALEMANY, A. 1993 The cylinder wake in a magnetic field aligned with the velocity. *J. Fluid Mech.* **253**, 421–448.

LIGHTHILL, M. J. 1963 Boundary layer theory. In *Laminar Boundary Layers* (ed. L. Rosenhead), pp. 46–113. Oxford University Press.

MATHAI, V., ZHU, X., SUN, C. & LOHSE, D. 2017 Mass and moment of inertia govern the transition in the dynamics and wakes of freely rising and falling cylinders. *Phys. Rev. Lett.* **119** (5), 054501.

MATHAI, V., ZHU, X., SUN, C. & LOHSE, D. 2018 Flutter to tumble transition of buoyant spheres triggered by rotational inertia changes. *Nat. Commun.* **9** (1), 1792.

MOREAU, R. J. 2013 *Magnetohydrodynamics*. Springer Science & Business Media.

MÜCK, B., GÜNTHER, C., MÜLLER, U. & BÜHLER, L. 2000 Three-dimensional MHD flows in rectangular ducts with internal obstacles. *J. Fluid Mech.* **418**, 265–295.

MUTSCHKE, G., GERBETH, G., SHATROV, V. & TOMBOULIDES, A. 2001 The scenario of three-dimensional instabilities of the cylinder wake in an external magnetic field: a linear stability analysis. *Phys. Fluids* **13** (3), 723–734.

NI, M.-J., MUNIPALLI, R., HUANG, P., MORLEY, N. B. & ABDOU, M. A. 2007 A current density conservative scheme for incompressible MHD flows at a low magnetic Reynolds number. Part II. On an arbitrary collocated mesh. *J. Comput. Phys.* **227** (1), 205–228.

PAN, J.-H., ZHANG, N.-M. & NI, M.-J. 2018 The wake structure and transition process of a flow past a sphere affected by a streamwise magnetic field. *J. Fluid Mech.* **842**, 248–272.

SCHWARZ, S., KEMPE, T. & FRÖHLICH, J. 2015 A temporal discretization scheme to compute the motion of light particles in viscous flows by an immersed boundary method. *J. Comput. Phys.* **281**, 591–613.

TCHOUFAG, J., FABRE, D. & MAGNAUDET, J. 2014 Global linear stability analysis of the wake and path of buoyancy-driven disks and thin cylinders. *J. Fluid Mech.* **740**, 278–311.

VELDHUIS, C. H. J. & BIESHEUVEL, A. 2007 An experimental study of the regimes of motion of spheres falling or ascending freely in a Newtonian fluid. *Intl J. Multiphase Flow* **33** (10), 1074–1087.

YONAS, G. 1967 Measurements of drag in a conducting fluid with an aligned field and large interaction parameter. *J. Fluid Mech.* **30** (4), 813–821.

ZHANG, C., ECKERT, S. & GERBETH, G. 2005 Experimental study of single bubble motion in a liquid metal column exposed to a DC magnetic field. *Intl J. Multiphase Flow* **31** (7), 824–842.

ZHANG, J. & NI, M.-J. 2017 What happens to the vortex structures when the rising bubble transits from zigzag to spiral? *J. Fluid Mech.* **828**, 353–373.

ZHENG, T. X., ZHONG, Y. B., LEI, Z. S., REN, W. L., REN, Z. M., DEBRAY, F., BEAUGNON, E. & FAUTRELLE, Y. 2015 Effects of high static magnetic field on distribution of solid particles in BiZn immiscible alloys with metastable miscibility gap. *J. Alloys Compounds* **623**, 36–41.

ZHOU, W. & DUŠEK, J. 2015 Chaotic states and order in the chaos of the paths of freely falling and ascending spheres. *Intl J. Multiphase Flow* **75**, 205–223.